eNeuro

Research Article: New Research | Disorders of the Nervous System

Electroconvulsive shock enhances responsive motility and purinergic currents in microglia in the mouse hippocampus

Alberto Sepulveda-Rodriguez[1,2], Pinggan Li[1,4], Tahiyana Khan[1,2], James D. Ma[1], Colby A. Carlone[1], P. Lorenzo Bozzelli[2,3], Katherine E. Conant[2,3], Patrick A. Forcelli[1,2] and Stefano Vicini[1,2]

[1]*Department of Pharmacology and Physiology, Georgetown University, Washington, DC, USA*
[2]*Interdisciplinary Program in Neuroscience, Georgetown University, Washington, DC, USA*
[3]*Department of Neuroscience, Georgetown University, Washington, DC, USA*
[4]*Department of Pediatrics, Sun Yat-Sen Memorial Hospital, Sun Yat-Sen University, Guangzhou, China*

https://doi.org/10.1523/ENEURO.0056-19.2019

Received: 13 February 2019

Accepted: 9 April 2019

Published: 15 April 2019

Author contributions: A.S.-R., P.A.F., and S.V. designed research; A.S.-R., P.L., T.K., P.L.B., K.C., P.A.F., and S.V. performed research; A.S.-R., P.A.F., and S.V. contributed unpublished reagents/analytic tools; A.S.-R., P.L., T.K., J.D.M., C.A.C., P.L.B., K.C., P.A.F., and S.V. analyzed data; A.S.-R., T.K., P.A.F., and S.V. wrote the paper.

Funding: Consejo Nacional de Ciencia y Tecnología (CONACYT)
381291
;

Funding: HHS | NIH | National Center for Advancing Translational Sciences (NCATS)
KL2 TR001432
;

Funding: HHS | NIH | Eunice Kennedy Shriver National Institute of Child Health and Human Development (NICHD)
R01 HD091994
;

Funding: HHS | NIH | National Institute of Neurological Disorders and Stroke (NINDS)
T32 NS041218
.

Conflict of Interest: Authors report no conflicts of interest.

NIH Grants KL2 TR001432 and R01 HD091994 to PAF; T32 NS041218 to PLB; CONACyT (Mexican Council on Science and Technology) Fellowship #381291 to AS.

Correspondence should be addressed to Stefano Vicini at svicin01@georgetown.edu.

Cite as: eNeuro 2019; 10.1523/ENEURO.0056-19.2019

1. Manuscript Title (50 word maximum):

Electroconvulsive shock enhances responsive motility and purinergic currents in microglia in the mouse hippocampus.

2. Abbreviated Title (50 character maximum):

μglia in mouse hippocampus respond to single ECS seizures.

3. List all Author Names and Affiliations in order as they would appear in the published article :

Alberto Sepulveda-Rodriguez[1,2], Pinggan Li[1,4], Tahiyana Khan[1,2], James D. Ma[1], Colby A. Carlone[1], P. Lorenzo Bozzelli[2,3], Katherine E. Conant[2,3], Patrick A. Forcelli[1,2] and Stefano Vicini[1,2]

[1]Department of Pharmacology and Physiology, [2]Interdisciplinary Program in Neuroscience and [3]Department of Neuroscience, Georgetown University, Washington DC, USA and [4]Department of Pediatrics, Sun Yat-Sen Memorial Hospital, Sun Yat-Sen University, Guangzhou, China.

4. Author Contributions: AS, PAF and SV conceived and designed the study; AS, PL, TK, PLB performed the experiments; AS, PL, JDM, CAC and PLB analyzed data; KEC contributed reagents and consulted on the project; AS, TK, PAF and SV prepared the figures and wrote the manuscript. All authors approved the final version of the manuscript.

5. Correspondence should be addressed to (include email address):

Stefano Vicini, Ph.D.
Dept. of Pharmacology & Physiology
Georgetown University Medical Center
3900 Reservoir Road NW, BSB225
Washington DC, 20007, USA
Email: svicin01@georgetown.edu
Office: 202-687-1567

6. Number of Figures: 8 7. Number of Tables: 0 8. Number of Multimedia: 0
9. Number of words for Abstract: 250 10. Number of words for Significance Statement: 117
11. Number of words for Introduction: 634 12. Number of words for Discussion: 1933

13. Acknowledgements: The authors would like to express gratitude for their useful discussions throughout this project to Drs. Kathleen-Maguire-Zeiss, John G. Partridge and Lindsay DeBiase, as well as the entire Vicini and Forcelli labs.

14. Conflict of Interest: A. No. Authors report no conflicts of interest.

15. Funding sources: NIH Grants KL2 TR001432 and R01 HD091994 to PAF; T32 NS041218 to PLB; CONACyT (Mexican Council on Science and Technology) Fellowship #381291 to AS.

ABSTRACT

Microglia are in a privileged position to both affect and be affected by neuroinflammation, neuronal activity and injury, which are all hallmarks of seizures and the epilepsies. Hippocampal microglia become activated after prolonged, damaging seizures known as Status Epilepticus (SE). However, since SE causes both hyperactivity and injury of neurons, the mechanisms triggering this activation remain unclear, as does the relevance of the microglial activation to the ensuing epileptogenic processes. In this study, we use electroconvulsive shock (ECS) to study the effect of neuronal hyperactivity without neuronal degeneration on mouse hippocampal microglia. Unlike SE, ECS did not alter hippocampal CA1 microglial density, morphology or baseline motility. In contrast, both ECS and SE produced a similar increase in ATP-directed microglial process motility in acute slices, and similarly upregulated expression of the chemokine CCL2. Whole-cell patch-clamp recordings of hippocampal CA1*sr* microglia showed that ECS enhanced purinergic currents mediated by P2X7 receptors in the absence of changes in passive properties or voltage-gated currents, or changes in receptor expression. This differs from previously described alterations in intrinsic characteristics which coincided with enhanced purinergic currents following SE. These ECS-induced effects point to a “seizure signature” in hippocampal microglia characterized by altered purinergic signaling. These data demonstrate that ictal activity *per se* can drive alterations in microglial physiology without neuronal injury. These physiological changes, which up until now have been associated with prolonged and damaging seizures, are of added interest as they may be relevant to electroconvulsive therapy, which remains a gold-standard treatment for depression.

SIGNIFICANCE STATEMENT

Epilepsy is the 4th most prevalent neurological disease, affecting 1 in 26 people over their lifetime. There is a critical unmet need in understanding basic mechanisms underlying the development of epilepsy (epileptogenesis), given that no disease-modifying treatments are currently available. How specific features of microglial activation contribute to subsequent epileptogenesis, and how seizure activity, per se, triggers changes in microglial responses is understudied. In this study, we demonstrate that hippocampal microglia react acutely to single non-epileptogenic seizures, in ways reminiscent of SE-induced activation. Thus, key features of the microglial activation pattern observed after SE may not be related to the epileptogenic process, and further work is needed to fully characterize the interplay between microglia, seizures and epilepsy.

INTRODUCTION

Neuroinflammation and microglial activation are hallmarks of many neurological and neurodegenerative diseases, including the epilepsies (Vezzani et al., 2011; Devinsky et al., 2013). As the resident immune macrophage population of the brain, microglia are in a privileged position to monitor neuronal health and activity, and to respond to neuronal injury or hyperactivity (Eyo et al., 2017). Beyond the traditional views of differential reactive microglial states leading to either pro- or anti-inflammatory signaling, microglia have distinct and well-established roles in critical components of development (Stevens et al., 2007; Tremblay et al., 2010), physiology (Tremblay et al., 2011; Schafer et al., 2013) and pathology (Hong et al., 2016; Vasek et al., 2016). These roles include synaptic pruning (Stevens et al., 2007) or displacement (Chen et al., 2014), neuronal phagocytosis (Fu et al., 2014) or trogocytosis (Weinhard et al., 2018), and neurotrophic support (Parkhurst et al., 2013).

It is now clear that microglia respond to epileptogenic insults in acquired models of epilepsy (Avignone et al., 2008, 2015; Shapiro et al., 2008; Menteyne et al., 2009; Ulmann et al., 2013; Arisi et al., 2015; Patterson et al., 2015; Rettenbeck et al., 2015; Sabilallah et al., 2016; Wyatt-Johnson et al., 2017; Kalozoumi et al., 2018; Klement et al., 2018). Furthermore, a recent study suggests that noninflammatory microglial changes could be the main driver of epileptogenesis in a mouse model of tuberous sclerosis (Zhao et al., 2018), although the specificity of the genetic tools used to target microglia in that study has been debated (Zou et al., 2017; Zhang et al., 2018).

Much like other epileptogenic insults to the brain (Klein et al., 2017), status epilepticus (SE) induces a wide spectrum of changes in pro- and anti-inflammatory cytokine expression and is accompanied by microglial proliferation and morphological/physiological activation (Avignone et al., 2008; Menteyne et al., 2009). Notably, SE triggers enhanced purinergic signaling in microglia, which correlates with increased velocity of microglial process motility (Avignone et al., 2008, 2015). (Ulmann et al., 2013). It is tempting to speculate that this response is an active contributor to the epileptogenic process. However, little is known about the effect of acute seizures/non-epileptogenic hyperactivity on these cells, making it imprudent to assume that they represent putative antiepileptogenic targets.

Moreover, because experimental SE in rodents also acutely causes extensive hippocampal degeneration (Turski et al., 1984; Pollard et al., 1994; Avignone et al., 2008) and blood-brain barrier breakdown (Marchi et al., 2007; van Vliet et al., 2007; Gorter et al., 2015), it is still unclear how much of the post-SE microglial activation is a result of the seizure activity *per se*, as opposed to the brain damage downstream of the epileptic crisis: it is plausible that the SE-induced injury (and not the SE itself) is the chief contributor to the particular SE-induced microglial activation.

To isolate the role of acute seizures from that of SE-induced damage, we used electroconvulsive shock (ECS), an acute seizure model that is not associated with epileptogenesis nor neuronal cell death (Orzi et al., 1990; Devanand et al., 1994; Scott, 1995; Conti et al., 2009; Basar et al., 2013; van Buel et al., 2017). Repeated ECS in rodents models human electro-convulsive therapy (ECT) with near-perfect validity (Li et al., 2007; van Buel et al., 2017). Above and beyond the established utility of

ECS in the preclinical screening of anti-seizure drugs, ECT is the most reliable and effective treatment for major depressive disorder (MDD) available in the clinic today (Group, 2003; Weiner and Reti, 2017). We found that hippocampal microglia responded to single ECS seizures with a striking upregulation of purinergic signaling and responsive process motility. Our new data are thus positioned to both address the role of acute hyperactivity-induced microglial activation in epilepsy, and also begin to unravel if hippocampal microglia participate in the mode of action of a *best-in-class* therapy against depression.

METHODS AND MATERIALS

Experimental Animals:

We used postnatal day (P)30-45 male and female $CX_3CR1^{GFP/+}$ mice, which possess green fluorescent protein in place of one allele of the fractalkine receptor gene, resulting in fluorescently labeled microglia (Jung et al., 2000). $CX_3CR1^{GFP/GFP}$ mice (#005582, RRID:IMSR_JAX:005582) were obtained from The Jackson Laboratory (Bar Harbor, ME, USA) and backcrossed onto a C57BL/6J (#000664, RRID:IMSR_JAX:000664) congenic background before this study. A total of 143 mice were used for the experiments in this study. All animals used in this study were housed on a standard 12:12 h light:dark cycle with water and standard chow available *ad libitum*.

Experimental and control mice were heterozygous littermates resulting from homozygote x wild type mating. Littermates were randomized to treatment and control groups. Matched control animals were handled and treated in the same manner except that they received sham/0mA shocks or saline/vehicle instead of pilocarpine injections (see below). Vehicle and sham control animals were pooled in a single control group for all analyses. The procedures described in this manuscript were performed with the approval of the Georgetown University Animal Care and Use Committee.

Maximal Electroshock:

Maximal (tonic-clonic) seizures were elicited by transcorneal stimulation using an Ugo Basile Electro-Convulsive Device (#57800, Stoelting Co., Wood Dale,

IL, USA) and custom-built transcorneal electrodes. Animals received 0.5% tetracaine HCl eyedrops (Alcon, Ft. Worth, TX, USA) 15-30 minutes before stimulation. Shocks consisting of 0.3s long trains of 0.9ms-wide square pulses (17mA for females, 19mA for males) at 200Hz reliably evoked a Tonic Hindlimb Extension (THE) response lasting between 12 and 20s with negligible mortality. Stimulation protocols and intensities were adapted from the literature (Frankel et al., 2001) and the associated Mouse Phenome Database (The Jackson Laboratory) dataset "Frankel1" publicly available online at https://phenome.jax.org/projects/Frankel1/protocol.

Status Epilepticus:

For the Status Epilepticus (SE) model (all injections were i.p. and all drugs were dissolved in sterile 0.9% NaCl unless noted otherwise): 30 minutes after pretreating with 1mg/kg each of scopolamine methylbromide and terbutaline (Cho et al., 2015), we injected 260-320mg/kg pilocarpine HCl;, and observed the animals as they progressed through modified Racine stages (1 = mouth and face automatisms, 2 = head bobbing, 3 = unilateral forelimb clonus, 4 = bilateral forelimb clonus and 5 = rearing and falling (Racine, 1972) and into SE (defined as continuous seizures over stage 3 for longer than 5 minutes). SE was terminated after 2h by injecting diazepam (10 mg/kg). Concurrently, mice received 0.25 mL (s.c.) of sterile warmed dextrose acetate Ringer's solution. Ethosuximide (150 mg/kg, s.c., in phosphate-buffered saline/PBS) was administered 6 hours after the start of seizures, together with 0.3mL of sterile 0.9% NaCl (Pearce et al., 2014; Iyengar et al., 2015). During and immediately after SE, mice were kept

192 huddled/touching in a bare warmed (30-31°C) cage. This induction protocol reliably
193 elicited SE in all our mice, with limited mortality (3/21 mice died during the
194 seizures).
195
196 Acute Slice Preparation:
197 24 hours following seizure induction, mice were euthanized by decapitation
198 and brains were rapidly dissected into an ice-cold sucrose aCSF slicing solution as
199 previously described (Al- Muhtasib et al., 2018), and in a manner consistent with
200 the AVMA guidelines on euthanasia of laboratory animals (AVMA, 2013). The slicing
201 solution contained (in mmol/L): 88 NaCl, 2.7 KCl, 0.5 $CaCl_2$, 6.6 $MgSO_4$ anhydrate,
202 1.4 NaH_2PO_4, 26 $NaHCO_3$, 25 dextrose and 75 sucrose (all chemicals from Sigma,
203 St. Louis, MO, USA unless otherwise noted). 300μm horizontal hippocampal slices
204 were cut on a Vibratome 3000 Plus Sectioning System (Vibratome, St. Louis, MO,
205 USA), in cold sucrose aCSF as above. Sections were recovered for 30 minutes at
206 32°C in normal/recording aCSF solution, containing in mmol/L: 124 NaCl, 4.5 KCl,
207 1.2 Na_2HPO_4, 26 $NaHCO_3$, 2 $CaCl_2$, 1 $MgCl_2$, and 10 dextrose. Slices were then
208 transferred to room temperature (RT = 22-24°C) and equilibrated for >10 minutes
209 before use. In some experiments, slices were incubated with 1.8μM sulforhodamine
210 101 in aCSF for 10 minutes to mark astrocytes (Nimmerjahn et al., 2004) for
211 unrelated studies (data not shown). To limit artifactual microglial activation from
212 dissection/sectioning, all slices were used within 5 hours of euthanasia, and all
213 microglia studied had somata at least 10μm away from the cut surfaces. aCSF
214 solutions were maintained at pH=7.4 by bubbling with carbogen gas (95% O_2 / 5%
215 CO_2, Roberts Oxygen, Rockville, MD, USA). All experiments were conducted at RT.
216

Patch Clamp Electrophysiology:

Whole-cell patch-clamp recordings were performed under DIC illumination on fluorescently identified ramified cells, with 4.5-6.5MΩ pipettes pulled from Wiretrol II borosilicate glass capillaries (Drummond, Broomall, PA, USA) filled with an internal solution as described in Avignone et al. 2008, containing (in mmol/L): 132 K-gluconate, 11 HEPES, 0.1 EGTA, and 4 $MgCl_2$, pH=7.35 adjusted with KOH.

Liquid junction potential (LJP = −14mV) was calculated in Clampex11 (pClamp, RRID:SCR_011323, Molecular Devices, San Jose, CA, USA). The LJP correction was only applied to our reported RMP values. Patch-clamp was performed with a MultiClamp700B amplifier (Molecular Devices). Recordings were digitized at 20kHz and low-pass Bessel-filtered at 2kHz with a personal computer running Clampex11 and a DigiData1440 (Molecular Devices).

Resting membrane potential (RMP) was measured in current clamp (I=0) mode, immediately after break-in to minimize effect of dialysis. All other data were recorded in voltage clamp configuration. Input resistance, access resistance and cell capacitance were calculated from the current response to brief −5mV hyperpolarizing voltage steps. I/V curves were calculated using 500ms voltage steps from −60mV to Vm = −120mV to +50mV, every 10mV.

For agonist-evoked current studies, cells were held at Vm = −60mV, with 500ms voltage ramps from −120mV to −50mV delivered every 10s. 1mM Na-ATP in normal or divalent cation-free/0CaMg aCSF (aCSF as described above, minus $CaCl_2$ and $MgCl_2$) was locally perfused via a custom-made Y-tube apparatus (Murase et al., 1989; Hevers and Lüddens, 2002). Recordings were analyzed offline with Clampfit 10.7 and 11.3 (pClamp, Molecular Devices). Results are shown as Current Density (C.D., in pA/pF) to take varying cell sizes/capacitances into account.

Access resistance was monitored periodically during the experiment and recordings with change greater than 20% were discarded.

For the P2X7 current studies, Brilliant Blue-G (BBG, #B0770, Sigma) was dissolved in aCSF to create a 1mM stock solution, and then some slices were preincubated in 5μM BBG in aCSF for 30 minutes (Avignone et al., 2008). Electrophysiology recordings were then conducted as outlined above but in the presence of 5μM BBG.

Confocal Imaging:

Confocal Z-or ZT-stacks were taken using a laser scanning microscope system (Thor Imaging Systems Division, Sterling, VA, USA) equipped with 488/561/642nm lasers and Green/Red/Far-red filters and dichroics and mounted on an upright Eclipse FN1 microscope (Nikon Instruments, Melville, NY, USA). 284x284x20μm (xyz) volumes of horizontal hippocampal slices containing CA1*sr* were imaged with a long working distance 60X water-dipping objective (CFI Fluor 60XW, NA=1.0, WD=2mm, Nikon). Differential interference contrast (DIC) images (on acute and fixed slices) or fluorescent images of NeuN (for neuronal nuclei) staining (on fixed slices only, see below) were used to identify and confirm our region of interest as CA1*sr*.

Microglial Motility:

For the baseline and responsive motility experiments, we took 1024x1024 pixel (px) ZT-stacks of acute slices by imaging 11 planes 2μm apart every 30s. If necessary, MIP (maximal intensity projections over the z-axis) timelapses were registered using the StackReg plugin (Thevenaz et al., 1998) in FIJI

(RRID:SCR_002285, Wayne Rasband/NIH, Bethesda, MD, USA) before the motility analyses.

Baseline Motility:

Spontaneous motility of microglial processes directly mediates the physical microglia-neuron contact that is a prerequisite for many microglial functions like phagocytosis of synaptic terminals. We imaged this baseline behavior over 20 minutes in CA1*sr* of either naïve slices or in the presence of a 0mM [ATP] containing (aCSF-only) pipette (controls for responsive motility, see below).

Motility analysis was performed in FIJI by adapting the method described in Eyo et al., 2018. We first manually cropped, then automatically thresholded and binarized the ROIs. The area above threshold at the end of the time-lapse movie (t=20 minutes) was then measured and normalized to the area above threshold of the first frame of the movie (t=0, extension index EI=1.0). The extension index through time of each time-lapse movie was then determined.

Responsive Motility:

Responsive motility of microglial processes is a vital endogenous response to injury (Davalos et al., 2005), and is a sensitive and reproducible in-slice assay of microglial purinergic signaling. In an assay adapted from the work of Avignone et al., 2008, we lowered a patch pipette containing 1, 3, or 10 mM [Na-ATP] in aCSF into CA1*sr*, 10-20µm deep, and imaged the volume surrounding it for 20 minutes. We quantified process velocity with the Manual Tracking plugin in FIJI (Cordelieres, 2018). Between 3-8 responding processes per slice were manually tracked as they moved towards the pipette. Control experiments with 0 mM ATP (aCSF only in the

pipette) did not elicit any appreciable directional motility in the processes of nearby microglia.

Tissue sectioning

Animals were anesthetized with unmetered isoflurane (Patterson Veterinary, Greeley, CO, USA) or pentobarbital (>100mg/kg) and intracardially perfused with cold PBS. Brains were quickly excised and drop-fixed overnight in 4% paraformaldehyde (#18505, Ted Pella Inc., Redding, CA, USA) + 4% sucrose in PBS. 50-100µm hippocampal slices were cut horizontally using a Vibratome Series 1000 (Vibratome) for immunostaining and morphometry. For FluoroJade C studies, fixed brains were cryoprotected overnight in 30% sucrose in PBS before freezing, and sectioned at 25µm on a cryostat (CM1850, Leica Biosystems, Nussloch, Germany) and immediately mounted on 10-12 gelatin-subbed slides per brain.

Microglial density:

For microglial density quantification we took 2048x2048 pixel Z-stacks of fixed slices from perfused brains by imaging 21 planes 1 µm apart. We analyzed the maximal intensity projections (MIPs) across the Z axis, referring to the 3D Z-stack for the manual cell counting analysis if necessary. Cells were manually counted using FIJI in a single 284x284x20 µm field containing CA1*sr* per hemi section.

Microglial morphology:

Following perfusion and sectioning, slices were processed free-floating for immunofluorescence against GFP to better visualize microglia and their fine

processes, and against NeuN to mark *stratum pyramidale*. Sections were blocked and permeabilized for 2 hours in 0.5% TritonX-100 and 10% normal goat serum in PBS. Next, slices were incubated overnight at 4°C with mouse anti-GFP (1:1000, Chemicon MAB3850, RRID:AB_94936, MilliporeSigma, Burlington, MA, USA) and rabbit anti-NeuN (1:500, ABN78, RRID:AB_10807945, MilliporeSigma). Slices were washed and then incubated at RT for 1 hour with secondary antibodies (1:1000 each; goat anti-mouse AlexaFluor647, #A-21235, RRID:AB_2535804, Thermo Fisher Scientific, Waltham, MA, USA; goat anti-rabbit Cy3, #111-165-144, RRID:AB_2338006, Jackson ImmunoResearch Laboratories, West Grove, PA, USA). Sections were mounted and coverslipped using VectaShield fluorescent mounting media (H-1200, RRID:AB_2336790, Vector Laboratories, Burlingame, CA, USA).

Individual microglia were traced using the "FilamentTracer" tool in Imaris 7.4.2 (RRID:SCR_007366, Bitplane, Concord, MA, USA) from Z-stacks of fixed anti-GFP stained slices with 41 planes of 4096x4096px taken at 0.5µm apart. We compared microglia morphometrically by extracting patterns of 3D Sholl crossings, numbers of branching points and primary branches, and total filament tree lengths for each traced cell.

FluoroJade C Staining:

To visualize neuronal damage, we used FluoroJade C, a polyanionic fluorescein derivative that can selectively mark degenerating neurons (Schmued et al., 2005). We employed an FJC Ready-to-Dilute kit (TR-100-FJC, Biosensis, Temecula, CA, USA) and followed the manufacturer's instructions, except for halving the time in potassium permanganate.

Briefly, after drying, slides were treated with basic ethanol solution for 5 minutes before transfer into 70% ethanol for 2 minutes, then rinsed in distilled/deionized water (ddH_2O) for 2 minutes. After incubating in a 0.06% potassium permanganate solution for 5 minutes, followed by a 2 min rinse in ddH2O, samples were stained in an acidified 0.001% FJC working solution for 10 minutes in the dark. After staining, slides were washed three times for 1 min in ddH2O, then placed on a slide warmer at 40°C until dry before being cleared in xylene for 2 minutes and coverslipped with D.P.X. mounting medium (#13510, Electron Microscopy Sciences, Hatfield, PA, USA). Fluorescence photomicrographs from 3-5 sections per slide were captured on an upright microscope (i80, Nikon Instruments, Melville, NY, USA) with a QIClick camera (QImaging, Surrey, B.C., Canada), using a standard FITC filter set and a 0.65NA 40X objective (Nikon Instruments). Images were captured by a blinded investigator using the same imaging conditions throughout. FJC positive cells in each image were manually counted by 2 blinded investigators. Cell counts were averaged from at least 3 sections per animal.

Microglial isolation:

Microglial isolation was performed 24 hours after ECS seizures, exploiting the Magnetic Activated Cell Sorting (MACS) approach with anti-Cd11b MicroBeads (#130-049-601, all MACS supplies are from Miltenyi Biotec, Gaithersburg, MD, USA), tightly adhering to the manufacturer's standard protocol for single cell dissociation and microglial isolation from adult brains, except for omission of the erythrocyte lysis step.

Mice were anesthetized and perfused transcardially with cold PBS. Brains were rapidly dissected on ice and stored in MACS Tissue Storage Solution (#130-100-008) until dissociation could proceed (less than 15 minutes). Brain tissues were sliced 6-8 times with a sterile scalpel, then placed together with the enzyme mix from the Adult Brain Dissociation kit (#130-107-677) in a C Tube (#130-093-237) for processing in the gentleMACS Octo Dissociator with Heaters (#130-096-427) using the recommended program (37C_ABDK_01). The dissociated tissue was resuspended in PBS and applied to a 30µm SmartStrainer (#130-098-458). All subsequent steps were performed at 4°C except for the magnetic column separation. The resulting single-cell suspension was centrifuged at 300g for 10 minutes at 4°C (Allegra X-30R, Beckman Coulter, Brea, CA, USA), and the supernatant aspirated. The cell pellet was resuspended in 3100µL of PBS and mixed with 900µL of Debris Removal Solution. 4mL of cold PBS was then overlaid on top, and the tubes were centrifuged for 10 min at 3000g. Three phases formed, the top two were discarded and cold PBS was added to the tube to bring the final volume to 15mL, before being centrifuged at 1000g for 10 minutes and aspirated completely. The pellet was resuspended in 10mL cold 0.5% BSA in PBS, and centrifuged at 300g for 10 minutes. The supernatant was again aspirated completely, and the cell pellet was carefully resuspended in 90uL cold 0.5% BSA, to which 10uL of MicroBeads were added before incubation in the dark for 15 minutes. The cells were washed in cold 0.5% BSA and centrifuged at 300g for 5 minutes, supernatant was aspirated completely, and the pellet was resuspended in 500uL 0.5% BSA. Microglia were magnetically isolated through MACS MS columns (#130-042-201) placed into MiniMACS Separator magnets (#130-042-102). Unlabeled cells were collected in the original flow-through and after 3x500uL

washes. Labeled microglial cells were collected by flushing the column after removal from the magnetic field.

RNA extraction and purification

After MACS isolation, positive fractions were immediately lysed with 0.8mL cold Trizol LS (Invitrogen #10296028, ThermoFisher Scientific) and homogenized by thorough pipette and vortex mixing. After a 5min initial incubation, 0.2mL chloroform (C7559, Sigma) was added and samples were incubated for 2-3 minutes before being centrifuged for 15 minutes at 12,000g and 4°C. The aqueous phase was transferred to a new tube with 0.5mL isopropanol (I9516, Sigma) and RNA was precipitated by incubating for 10 minutes at RT. After being centrifuged for 10 minutes at 12,000g and 4°C, the supernatant was discarded, and the RNA washed twice by resuspending the pellet in 75% ethanol (E7023, Sigma) in UltraPure Nuclease-free ddH_2O (Invitrogen #10977023, ThermoFisher Scientific), then vortexing briefly and then spinning down for 5 minutes at 7,500g and 4°C. After the 2nd wash was removed, RNA was air-dried for 10 minutes before resuspension in 25µL RNase-free water. Samples were then incubated at 60°C for 10-15 minutes before RNA quantity and purity were determined by standard spectrophotometry methods (NanoDrop 1000, ThermoFisher Scientific). If necessary, RNA samples were stored at -80°C before cDNA synthesis and qPCR analysis downstream.

mRNA expression analysis by 2-step RT-qPCR

cDNA was synthesized from RNA samples using random hexamer primers in the SuperScript IV First Strand Synthesis system (Invitrogen #18091050,

ThermoFisher Scientific) according to the manufacturer's directions. cDNA samples were stored at -20°C before qPCR analysis. 10% of the 20µL RT reaction output was used in a 20µL qPCR reaction for each technical replicate.

Hydrolysis probe-based qPCR reactions were run in multiplex on a 4-channel (FAM,HEX,TEX615,Cy5) Mic cycler instrument (Bio Molecular Systems, Upper Coomera, Australia) using mouse assays from the PrimePCR line (Bio-Rad, Hercules, CA, USA) as follows (with format *Gene*: Unique AssayID): *Actb*: qMmuCEP0039589; *Tmem119*: qMmuCEP0042925; *Tnf*: qMmuCEP0028054; *Ccl2*: qMmuCEP0056726; *P2rx1*: qMmuCIP0031612; *P2rx4*: qMmuCIP0028782; *P2rx7*: qMmuCIP0042331; *P2ry6*: qMmuCIP0029813; *P2ry12*: qMmuCEP0057087.

PCR reactions were prepared in duplicate or triplicate with Bioline SensiFast Probe No-ROX mastermix (Thomas Scientific, Swedesboro, NJ, USA) following the manufacturer's directions for multiplex assays (polymerase activation for 3 minutes @ 95°C; then 40 cycles of 10s denaturation @ 95°C, 50s annealing/extension @ 60°C, signal acquisition). Multiplex assay combinations were validated by comparing their results to those from parallel singleplex reactions (data not shown). Threshold cycle was automatically determined and averaged across replicates by the cycler manager software (Bio Molecular Sciences). Fold changes were determined using the $2^{-\Delta\Delta Ct}$ method, with expression of all transcripts normalized to *Actb* levels in the control group.

<u>CCL2 ELISA and total protein quantification on hippocampal lysates:</u>

After decapitation, hippocampi were dissected in ice-cold PBS, flash frozen in isopentane cooled in dry ice (−78°C), and lysed (200µL of RIPA buffer + HALT inhibitor cocktail/hemi-hippocampus, both from ThermoFisher Scientific). Lysates

were probed for total protein using a Pierce BCA assay (#23227, ThermoFisher Scientific) and for CCL2/MCP-1 using a Quantikine CCL2 ELISA (MJE00, R&D Systems, Minneapolis, MN, USA) assay according to manufacturers' directions.

Experimental Design and Statistical Analysis:

Our primary question of interest was the degree to which ECS would alter microglial responses. The impact of SE on the same endpoints we measure for ECS have been previously reported and replicated by others (Avignone et al., 2008, 2015; Menteyne et al., 2009; Eyo et al., 2014, 2016; Arisi et al., 2015; Schartz et al., 2016; Tian et al., 2017; Wyatt-Johnson et al., 2017). For comparison purposes, we included a Status Epilepticus group as a positive control in subset of experiments. We focused our analysis on CA1, as the microglial response to status epilepticus has been best characterized in this region. All data were analyzed by investigators blinded to treatment status using FIJI, Clampfit 10.7 and 11, Excel (RRID:SCR_016137, Microsoft, Redmond, WA, USA) and Prism (RRID:SCR_002798, GraphPad, LaJolla, CA, USA). Results are presented as mean±Standard Error of the Mean (SEM). N is number of animals and n is number of slices/fields or number of cells for the patch-clamp electrophysiology studies. We did not detect any sex differences in microglial density, morphology and motility, or in microglial gene expression, and thus combined data across sexes for further statistical analysis. Similarly, wherever applicable, control groups for both seizure models (saline vehicle for SE, sham shock for ECS) were combined.

Data were statistically analyzed by two-way ANOVA followed by Sidak's multiple comparisons test (microglial 3D Sholl analysis data/Fig. 3B; qPCR data/Fig. 4B/Fig. 8), by one-way ANOVA followed by post-hoc multiple

comparisons with Tukey's test (other microglial morphometry data/Figs. 3C,D,E; CCL2 ELISA analysis data/Fig. 4A), by Kruskal-Wallis non-parametric test followed by multiple comparisons with Dunn's correction (for the non-normally distributed BBG preincubation electrophysiology data, Figs. 7E,F), or by unpaired t-tests for all other comparisons. We established statistical significance at $p < 0.05$, applied recommended multiple comparison corrections where appropriate and computed all p-values from two-tailed distributions. Exact p-values are provided whenever made available by the statistics software (Prism).

474

475 **RESULTS**

476 To characterize the microglial response to neuronal hyperactivity/seizures
477 we employed electroconvulsive shock to induce maximal seizures on $CX_3CR1^{GFP/+}$
478 mice and studied green fluorescent protein-labeled microglia in hippocampal area
479 CA1*sr*.

480 A single ECS-induced tonic-clonic seizure did not result in observable
481 differences in microglial density or baseline motility 24 hour after the seizures in the
482 CA1sr hippocampal region. As shown in the examples in Fig. 1A and the summary
483 data in Fig. 1B (by slice/field), CA1 slices from control animals (N=13 mice, n=56
484 fields) had a mean cell density of 27±2.9 microglia /10^6 μm^3 of volume imaged,
485 compared to 28±2.7 in the ECS group (N=12, n=53) (by slice: $t_{(107)}$=0.949, p=0.34,
486 t-test; by animal: $t_{(23)}$=0.367, p=0.717, t-test, data not shown).

487 To verify that our ECS treatment was not associated with neuronal damage
488 in the hippocampus, we counted FluoroJade C (FJC) positive cells. FJC is a
489 polyanionic dye that selectively marks degenerating neurons (Schmued et al.,
490 2005). The number of FJC+ cells per 320μm x 240μm field imaged was low in
491 controls (4.2±0.36; N=9) and ECS-exposed animals (3.6±0.54; N=5), but
492 significantly elevated in animals that underwent SE (16.3±1.5; N=7, Fig. 1C).
493 Analysis by one-way ANOVA revealed a statistically significant effect of treatment
494 ($F_{(2,18)}$=53.1, p=0.00000003), that was driven by the SE group, which differed from
495 both control ($q_{(18)}$=13.13, p=0.00000008, Tukey's test) and ECS groups
496 ($q_{(18)}$=11.89, p=0.0000003, Tukey's test). Control and ECS groups did not differ
497 from each other ($q_{(18)}$=0.612, p=0.902, Tukey's test). Thus, as expected, single

ECS did not cause acute neurodegeneration, a profile different from that following SE, which is associated with high levels of degeneration.

To evaluate baseline motility, we calculated an extension index by dividing the mean area of process extensions by the mean area of retracted processes (Eyo et al., 2018) over an imaged field as shown in the examples in Figs. 2A and 2B. Over 20 minutes of imaging under baseline conditions, we measured similar mean extension indices of 1.09±0.04 for control slices and 1.07±0.05 for ECS slices (N=7 and 6 animals; n=17 and 12 slices; $t_{(27)}$=0.269, p=0.79, t-test, Fig. 2C).

To investigate the effect of our experimental treatment on microglial morphology we reconstructed confocal z-stacks of individual cells in CA1*sr* after perfusion, fixation, and immunofluorescent amplification of GFP. Representative tracings are shown in Figure 3A. We traced a total of 14 cells from 7 control animals, 14 cells from 7 ECS animals, and 10 cells from 5 SE animals.

Microglia from control animals were highly ramified and had long and complex processes with regular branching, as is expected under physiological conditions. Compared to controls, and unlike ECS animals, SE animals displayed clear morphological activation of hippocampal microglia, as has been previously described by others (Avignone et al., 2008, 2015; Wyatt-Johnson et al., 2017). The 3D Sholl profile was more compact in slices from SE-exposed animals as compared to slices from controls ($F_{(1,1320)}$=1761, $p<10^{-15}$), with significantly fewer crossings from 2μm to 33μm from the cell body (all p<0.0001, Tukey's multiple comparisons tests, Fig. 3B). Cells from SE-exposed animals had a significantly shorter total process length (748±44μm in control vs. 178±26μm in SE, $q_{(35)}$=13.4, p=0.0000000001, Tukey's test, Fig. 3C), and also had significantly fewer branching

points (68±4.2 in control vs. 9.4±2.0 in SE, $q_{(35)}$=12.4, p=0.0000000007, Tukey's test, Fig. 3D) and primary branches (9.5±0.53 in control vs. 3.7±0.42 in SE, $q_{(35)}$=12.73, p= 0.0000000004, Tukey's test, Fig. 3E). On the other hand, microglia from the hippocampus of ECS-exposed animals had no detectable differences in morphology when compared to controls. Their 3D Sholl profile was similar to control cells (p>0.9 at all radii, Tukey's multiple comparisons tests, Fig. 3B), and they also had comparable total process length (843±43μm, $q_{(35)}$=2.422, p=0.22, Tukey's test, Fig. 3C), and number of branching points (76±5.5, $q_{(35)}$=1.79, p=0.43, Tukey's test, Fig. 3D) and primary branches (8.36±0.31, $q_{(35)}$=2.747, p=0.142, Tukey's test, Fig. 3E).

Thus, ECS did not induce any observable microglial activation as measured by microglial density, spontaneous motility or morphology. Given that "activated" microglia are at once a result, target, and source of proinflammatory molecules, we wanted to verify that our model was associated with low relative expression levels of CCL2 (also known as MCP-1), a chemokine whose expression was significantly upregulated after SE (Avignone et al., 2008; Foresti et al., 2009; Arisi et al., 2015). CCL2 has been mechanistically implicated in the neuronal cell death that follows Status Epilepticus (Tian et al., 2017).

Surprisingly, as shown in Fig. 4A, ECS and SE induced a similar increase in CCL2 protein levels as measured by ELISA in hippocampal lysates taken 24 hours after the seizures. As expected, lysates from control animals displayed low levels of CCL2 (0.9±0.12 pg CCL2/mg total protein; N=16 hippocampi from 16 animals). One-way ANOVA revealed a statistically significant treatment group effect ($F_{(2,32)}$=6.13, p=0.0056). This effect was driven by a significant increase in CCL2 in

546 the ECS (1.6±0.18pg/mg total protein, N=11, $q_{(32)}$=4.48, p=0.0091) and SE
547 (1.5±0.27pg/mg total protein, N=8, $q_{(32)}$=3.61, p=0.041) groups, as compared to the
548 control group by Tukey's test. There was no significant difference in CCL2 protein
549 expression between the ECS and the SE groups ($q_{(32)}$=0.416, p=0.95). When
550 microglial RNA samples were analyzed by qPCR, two-way repeated measures
551 mixed model ANOVA analysis showed significant effects of treatment group
552 ($F_{(1,28)}$=5.311, p=0.03), interaction between treatment group and gene
553 ($F_{(2,28)}$=5.815, p=0.008) as well as of gene assayed ($F_{(2,28)}$=5.156, p=0.01). As
554 shown in Fig. 4B, we found *Ccl2* to be significantly changed: in accordance with the
555 increased CCL2 protein expression in ECS hippocampi (see Fig. 4A), *Ccl2* mRNA
556 levels were significantly upregulated in ECS microglia compared to controls (control
557 FC = 1.07±0.18, ECS FC = 3.56±0.97, $t_{(28)}$=3.959, p=0.001, N=5/group). No
558 differences were found in relative expression of the microglial marker *Tmem119*
559 (control FC = 1.01±0.07, ECS FC = 0.91±0.07, $t_{(28)}$=0.175, p>0.99, N=6/group) or
560 the pro-inflammatory cytokine *Tnf* (control FC = 1.43±0.45, ECS FC = 1.41±0.25,
561 $t_{(28)}$=0.039, p>0.99, N=6/group).

562 CCL2 signaling is extensively intertwined with epilepsy, simultaneously
563 serving as a cause *and* consequence of both neuronal hyperexcitability and injury
564 (Bozzi and Caleo, 2016). Indeed, besides the connection to post-SE injury noted
565 above, CCL2 has been implicated in the seizure-promoting effects of systemic
566 inflammation (Cerri et al., 2016), and has also been shown to directly upregulate
567 microglial purinergic signaling (Toyomitsu et al., 2012). Given the surprising ECS-
568 induced increase in CCL2 expression, we next tested for one of the more distinctive
569 facets of the purinergic signaling changes seen in SE-induced microglial activation:

570 the enhancement of microglial responsive motility (Avignone et al., 2008, 2015).
571 Motility of microglial processes across increasing ATP gradients (and towards point
572 sources of extracellular ATP, from diffusion) is an important endogenous response
573 to injury (Davalos et al., 2005), as well as a sensitive in-slice assay of microglial
574 purinergic signaling.

575 We thus next investigated the effect of ECS on this microglial behavior, by
576 imaging process extension and migration responses to a pipette containing ATP in
577 aCSF (Figs. 5A,B). As summarized in Fig. 5C, microglia from control animals slowly
578 mounted a response in the form of a narrowing circle, formed by the leading edge
579 of the processes as they advanced towards the pipette. Importantly, this directional
580 motility was not evoked by 0mM [ATP]/aCSF-only pipettes, suggesting that the
581 response was purely to ATP and not to the physical presence of the pipette.

582 In stark contrast to the responses in control slices, slices from ECS and SE
583 animals displayed similarly enhanced microglial process motility towards 3mM ATP
584 in a patch pipette, 24 hours after the seizures. One-way ANOVA revealed a
585 significant effect of treatment group ($F_{(2,91)}=17.9$, $p<10^{-15}$). Control slices (n=39
586 slices from N=10 animals) displayed a mean process velocity of 2.7±0.04μm/min,
587 compared to 4.3±0.12μm/min for 38 slices from 10 ECS animals, and
588 4.4±0.23μm/min for 17 slices from 5 SE animals (by Tukey's multiple comparison
589 test; C vs. ECS: $q_{(91)}=15.7$, p=0.0000000004; C vs. SE: $q_{(91)}=13.1$,
590 p=0.0000000004; ECS vs. SE: $q_{(91)}=0.793$, p=0.84). ECS enhancement of ATP-
591 directed microglial process motility was relatively much smaller but still statistically
592 significant when the concentration of ATP in the patch pipette solution was 1mM
593 (1.5±0.05μm/min for control vs. 1.8±0.05μm/min for ECS, $t_{(18)}=3.79$, p=0.0013, t-

test, n=10 slices per group, from N=3 animals per group). A difference between groups was not detectable when the pipette contained a saturating concentration of ATP (10mM; 5.3±0.14μm/min for control vs. 5.4±0.17μm/min for ECS, $t_{(17)}$=0.233, p=0.82, t-test, n=10 and 9 slices per group, from N=3 animals per group).

Because we did not observe a change in microglial morphology or spontaneous motility, and the effect of ECS on responsive motility was occluded at the highest ATP concentration, our data suggest that ECS increases purinergic responses within microglia, rather than increasing endogenous ATP release activity guiding microglia.

To directly test the hypothesis that ECS enhanced purinergic signaling mechanisms in microglia, and to further characterize hippocampal microglia after ECS, we used patch-clamp electrophysiology targeting fluorescently tagged microglia (Fig.6) as had previously been done after SE (Avignone et al., 2008). As measured by whole-cell recordings in acute hippocampal slices, control microglia displayed the expected negligible voltage-activated currents, bi-modal distribution of negatively polarized resting membrane potentials, high input resistance, and relatively low capacitance. ECS did not affect the intrinsic electrophysiological properties of CA1*sr* microglia: we did not detect any induction of Kv voltage-activated potassium currents or changes in I/V curves in the voltage range tested (effect of treatment group: $F_{(1,468)}$=0.165, p=0.69, two-way ANOVA, Fig. 6B, n=16 and 12 cells), and the distributions of resting membrane potential ($t_{(29)}$=0.635, p=0.53, t-test, Fig. 6C, n=17 and 14), input resistance ($t_{(32)}$=0.348, p=0.73, t-test, Fig. 6D, n=20 and 14) and membrane capacitance ($t_{(33)}$=1.02, p=0.316, t-test, Fig. 6E, n=21 and 14) were all similar across both groups (N=3 and 4 mice for the control and ECS groups respectively) and in accordance with published ranges

(Avignone et al., 2008; Menteyne et al., 2009; Kettenmann et al., 2011; Verkhratsky and Noda, 2014; de Biase et al., 2017; Madry et al., 2018).

Local perfusion of 1mM Na-ATP through a Y-tube application device rapidly and reproducibly evoked inward currents in cells from control slices which reversed near 0mV and were potentiated by divalent cation-free aCSF, putatively identifying them as cationic purinergic currents mediated by P2X receptors (Khakh et al., 2001; Jarvis and Khakh, 2009). ECS significantly increased the current density of the response under both conditions, as illustrated in the example traces in Figs. 7A,B and summarized in Figs. 7C,D. In normal aCSF, control cells had a mean current density of 0.152±0.052 pA/pF in response to 1mM ATP when held at Vm = −60mV, which was significantly smaller than the 0.596±0.073 pA/pF in ECS cells ($t_{(18)}$=5.07, p=0.000079, t-test, Fig. 7C, n=12 and 8). In divalent cation-free aCSF, control cells had a mean evoked current density of 5.02±1.28 pA/pF, which was significantly smaller than the 11.6±1.62 pA/pF in ECS cells ($t_{(21)}$=3.23, p=0.0041, t-test, Fig. 7D, n=12 and 11).

Next, we sought to identify the receptors underlying these enhanced currents by preincubation of slices with the purinergic inhibitor Brilliant Blue G/BBG (5 μM) which preferentially blocks P2X7 over P2X4 and P2X1 (Jiang et al., 2000). Microglia in BBG-treated slices from both control and ECS-treated animals failed to display a current response to 1mM ATP in normal aCSF (n=6 and 11 cells from N=2 animals/group, Fig. 7E, Kruskal-Wallis test, $H_{(3)}$=27.8, p=0.000004). This was particularly striking in the ECS group, where we detected measurable currents in all cells incubated in normal ACSF and failed to detect any response in cells from slices incubated with BBG. Multiple comparisons tests revealed a significant

643 decrease in current density between ECS cells incubated in aCSF vs. those
644 incubated in BBG (Dunn's test, p=0.000002). Given that the currents evoked in
645 control slices incubated with aCSF were small (and only detectable in half the cell
646 we recorded from), this group did not differ following incubation in BBG (Dunn's
647 test, p=0.411).

648 Similarly, as summarized in Fig. 7F, BBG preincubation drastically reduced
649 the current density elicited by 1mM ATP in 0CaMg/divalent cation-free aCSF: we
650 recorded mean responses of 0.156±0.073 pA/pF for 6 cells from 2 control animals
651 and 0.92±0.38 pA/pF for 10 cells from 2 ECS animals (Kruskal-Wallis test,
652 $H_{(3)}$=29.9, p=0.000001). Multiple comparisons tests revealed significant differences
653 in ATP-evoked current densities from: cells from control slices exposed to BBG
654 versus those that weren't BBG-treated (Dunn's test, p=0.0052) and cells from ECS
655 slices exposed to BBG versus those that incubated in control aCSF (Dunn's test,
656 p=0.00002). These findings are consistent with higher affinity, larger conductance,
657 or increased number of P2X7-containing receptors in hippocampal microglia post-
658 ECS.

659 We next sought to quantify the relative expression of various purinergic
660 receptor genes in microglia after ECS. As illustrated in Fig. 8, the above described
661 changes in microglial purinergic function were not accompanied by increases in
662 expression of receptor mRNA, as measured by qPCR: two-way repeated measures
663 mixed model ANOVA analysis showed no effect of treatment group ($F_{(1,25)}$=2.213,
664 p=0.149), of interaction between treatment group and gene ($F_{(4,25)}$=1.377, p=0.270)
665 or of gene assayed ($F_{(4,25)}$=0.8903, p=0.484). There were no statistical differences
666 in relative expression between control and ECS microglial samples (all evaluated

667 by Sidak's test for multiple comparisons) for: *P2rx1* (control FC = 1.02±0.08, ECS
668 FC = 1.05±0.15, $t_{(25)}$=0.2205, p>0.99, N=6/group), *P2rx4* (control FC = 1.02±0.08,
669 ECS FC = 1.09±0.16, $t_{(25)}$=0.4724, p>0.99, N=6/group), *P2rx7* (control FC =
670 1.05±0.14, ECS FC = 0.66±0.15, $t_{(25)}$=2.476, p=0.102, N=6/group), *P2ry6* (control
671 FC = 1.05±0.15, ECS FC = 1.06±0.13, $t_{(25)}$=0.5179, p>0.99, N=6/group), or *P2yr12*
672 (control FC = 1.00±0.01, ECS FC = 0.83±0.16, $t_{(25)}$=1.026, p>0.99, N=6/group). The
673 lack of changes in transcript levels suggest that translational or posttranslational
674 alterations account for the enhanced P2X7 dependent currents we observed after
675 ECS.
676

DISCUSSION

Here we report a spectrum of changes in hippocampal microglia in response to maximal electroconvulsive shock seizures (ECS). This ECS-induced "activation" state features changes that partially overlap with those seen after status epilepticus. ECS (unlike SE) did not cause observable differences in hippocampal microglial proliferation/density, morphology, spontaneous motility, or intrinsic electrophysiological properties. On the other hand, similarly as after SE, ECS resulted in increased gene and protein expression of *Ccl2*/CCL2, a chemokine with an established role in neuron-glia-inflammation crosstalk in healthy states and in seizures/epilepsy. Moreover, ECS enhanced ATP-responsive motility and ATP-evoked currents in microglia, in the absence of measurable changes in receptor expression. Thus, brief, non-injurious seizures (ECS) partially recapitulate the activation state seen after prolonged, injurious seizures (SE). This overlap suggests that for a subset of features, seizure activity *per se*, and not neuronal damage, drives microglial responses.

A potential concern raised regarding evaluation of microglia in acute brain slices is that the slicing process itself may alter microglial state or response. Following others (Avignone et al., 2008), we employed the protective cold sucrose slicing technique and used slices within five hours or less after slicing. Slices from control and ECS animals deteriorated in a similar fashion, as approximated by the ease of obtaining patch-clamp recordings from ramified GFP^+ cells deep in the slice and the quality of those recordings. Moreover, our findings with SE mirror those previously reported by others using multiple slice preparation approaches. It does remain possible that either ECS or SE makes neurons more vulnerable to the slicing

protocol, meaning that some of our observations could arise from a seizure/slicing interaction.

Commonly employed chemoconvulsant-induced SE models are associated with severe damage in the hippocampus (Turski et al., 1984; Covolan and Mello, 2000), above and beyond the sclerosis associated with the human epilepsies (Löscher, 2011; Becker, 2017). As such, it remains plausible that parts of the SE-induced changes in hippocampal microglia are in fact an acute response to the extensive neuronal injury. Our data seem to support this idea; ECS, which is neither epileptogenic nor damaging induced only a subset of features seen after SE. Thus, the marked proliferation, morphological simplification, enhancement of baseline motility and changes in intrinsic electrophysiological properties observed in hippocampal microglia after SE but not after ECS may be a response to damage. This would be consistent with the canonical pro-inflammatory role of microglia after injury to the healthy brain (Nimmerjahn et al., 2005). The reported time course and anatomical profile of the microglial response to SE lend additional credence to this correlation, since the changes in proliferation and morphology after SE are localized to areas and time periods where neuronal cell death is expected (Covolan and Mello, 2000; Wyatt-Johnson et al., 2017). Furthermore, SE models relying on systemic or local chemoconvulsant application could additionally be having direct drug effects on the microglia, although single microglia do not express kainate or muscarinic receptors (Hammond et al., 2018; McCarroll and Stevens, 2018). This potential confound is mostly mitigated by the finding that different models of SE induction are associated with similar microglial activation (Avignone et al., 2008;

Menteyne et al., 2009; Eyo et al., 2014; Arisi et al., 2015; Avignone et al., 2015; Eyo et al., 2016b; Schartz et al., 2016; Tian et al., 2017; Wyatt-Johnson et al., 2017).

On the other hand, our data also show that the microglial responses to ECS and SE have characteristics in common. Both models similarly enhanced the velocity motility of microglial processes in response to a local source of ATP in slices, a sensitive functional assay of P2Y12 receptor signaling in microglia, since this is the receptor underlying the process extensions (Haynes et al., 2006; Ohsawa et al., 2010).

Since the ECS-induced increase in velocity was not detected in response to saturating ATP concentrations, this suggests changes in number or function of purinergic receptors in microglia, as opposed to ambient ATP levels or ATP-induced ATP release from astrocytes. This is noteable, given that multiple groups have reported increased ATP levels after brain stimulation (Wu and Phillis, 1978; Wieraszko et al., 1989). Conversely, adenosine, which mediates microglial process retraction (Orr et al., 2009), is also increased in the brain after seizures (Ilie et al., 2012; Lovatt et al., 2012). Interestingly, our whole-cell patch-clamp experiments on microglia in hippocampal slices from ECS-exposed animals also showed a greater P2X current density, chiefly mediated by P2X7-containing receptors. These channels possess biophysical characteristics like calcium permeability and conductance sensitization/pore size increase (Liang et al., 2015) that likely underlie their well-established roles in epilepsy and neuroinflammation (Henshall and Engel, 2015; Amhaoul et al., 2016; Beamer et al., 2017). Since directed motility in response to ATP is the first phase of the microglial response to neuronal injury (Davalos et al., 2005), and P2X7 receptors have a role in the ensuing neuroinflammation, it seems

748 that the seizures in both of our studied models are priming microglia to mount both
749 a faster and stronger response to future insults.

750 We failed to detect any differences in passive properties (resting membrane
751 potential/RMP, input resistance/IR or membrane capacitance/Cm) or in voltage-
752 activated currents following ECS. These data are consistent with the lack of an
753 effect on morphology and baseline motility, since IR and Cm directly reflect cell
754 membrane properties, and changes in voltage-activated potassium currents
755 underlie pathogenic microglial-neuron contacts resulting in cell death after SE
756 (Fordyce et al., 2005; Menteyne et al., 2009). Thus, our results point to parallel
757 enhancements in metabotropic and ionotropic purinergic signaling within
758 hippocampal microglia after ECS, in the absence of changes in morphology,
759 baseline motility or intrinsic electrophysiological characteristics. In this way, one
760 can reimagine the complex SE-induced activation state as comprising a particular
761 response to seizures, as well as a parallel response to neuronal injury.

762 CCL2 (C-C motif chemokine ligand 2, also known as monocyte chemoattractant
763 protein 1 or MCP-1) is a canonically pro-inflammatory signaling molecule that has
764 been strongly implicated in the post-SE neuronal injury (Foresti et al., 2009; Arisi et
765 al., 2015; Bozzi and Caleo, 2016; Tian et al., 2017) as well as in the seizure-enhancing
766 effects of systemic inflammation (Cerri et al., 2016). Unexpectedly, given the lack of
767 neuronal damage (and epileptogenesis) after ECS as compared to SE, we detected
768 similarly increased CCL2 protein expression in hippocampal lysates from our ECS-
769 exposed animals. In accordance with this finding, we also observed significantly
770 higher expression of *Ccl2* mRNA in microglia after ECS. This change was not
771 accompanied by increased levels of *Tnf* mRNA, another pro-inflammatory cytokine

772 whose expression is increased post-SE (Avignone et al., 2008). Interestingly,
773 upregulated TNF signaling is thought to underlie the pathogenic losses in blood-
774 brain barrier integrity described after SE (Marchi et al., 2007; Kim et al., 2013; Klement
775 et al., 2018). Although the protein experiments were performed on hippocampal
776 lysates obtained from rapid decapitation without transcardial perfusion, where
777 contamination from blood could cloud our analysis, the qPCR data is derived from
778 MACS-purified microglial samples from perfused animals, strengthening our
779 conclusion.

780 SE, inflammation, and subsequent injury/epileptogenesis are intricately linked
781 through at least two related signaling pathways: fractalkine and interleukin 1-beta.
782 Neuronal-microglial fractalkine signaling, and subsequent astrocytic and neuronal
783 IL-1R activation have been extensively implicated in the pathogenesis mechanism
784 observed after SE (Ravizza and Vezzani, 2005; Ali et al., 2015; Eyo et al., 2016a; Tian et
785 al., 2017), as well as in other rodent models of acquired epilepsy (Plata-Salamán et al.,
786 2000).

787 Besides complicating the picture as far as the role of CCL2 in neuronal injury
788 post-SE, our finding of increased hippocampal CCL2/microglial *Ccl2* after ECS is of
789 particular interest given the fact that this chemotactic cytokine has been found to
790 directly enhance purinergic signaling in microglia by promoting trafficking of
791 receptors like P2X4 to the microglial plasmalemma (Toyomitsu et al., 2012); whether
792 CCL2 influences trafficking of other receptors such as P2X7 is unknown. However,
793 by some reports, microglial as well as neuronal P2X7 levels are increased in TLE
794 patients and rodent SE models (Jimenez-Pacheco et al., 2013), while transient

795 inhibition of P2X7 resulted in lasting decreases of post-SE neurodegeneration,
796 gliosis and epileptogenesis (Engel et al., 2012; Jimenez-Pacheco et al., 2016).
797 Unlike the observed increase in CCL2 protein levels which is correlated with an
798 increase in *Ccl2* mRNA abundance, the increases in purinergic receptor function
799 could not be explained by changes in microglial gene expression. Indeed, we
800 observed no significant differences in microglial expression of *P2rx1*, *P2rx4*, *P2rx7*,
801 *P2ry6* and *P2ry12* mRNAs post-ECS. Notably, while SE models seem to robustly
802 change the number, morphology and purinergic physiology of hippocampal
803 microglia, the effect of SE on purinergic gene expression has incited controversy in
804 the field and seems to depend not only on timing, strain, age, and model, but also
805 on laboratory. For instance, different groups have reported unchanged (Bosco et al.,
806 2018), decreased (Alves et al., 2017) and increased (Avignone et al., 2008) expression
807 of purinergic receptor gene *P2ry12* in the latent phase of similar models of SE.
808 Likewise, the transcript for *P2rx7* has been reported as both being increased
809 (Avignone et al., 2008; Jimenez-Pacheco et al., 2016) and unaffected (Bosco et al., 2018)
810 post-SE. Thus, the direction and even existence of an SE-induced effect on
811 expression of purinergic receptor genes remains controversial. While a change in
812 microglial expression of *P2rx7* would have been the most parsimonious explanation
813 for the increased P2X7 current density, several possibilities, including biophysical
814 and/or pharmacological changes in the P2X7 channel properties could explain
815 these findings and will have to be further investigated.
816 Other published work has studied the microglial response after ECS (Jinno and
817 Kosaka, 2008; Jansson et al., 2009), but only found significant changes in microglial
818 density and morphological/functional activation after chronic ECS stimulation (10-

30 seizures). Concordant with our present study, one of these previous studies found that single ECS seizures failed to elicit changes in number or morphology of microglia (Jinno and Kosaka, 2008).

While SE and ECS seizures clearly manifest differently in EEG and behavioral measures, both types of seizures have been shown to recruit the hippocampal formation (INGVAR, 1986; Morinobu et al., 1997; Hsieh et al., 1998; Ji et al., 1998; Scorza et al., 2002; Dyrvig et al., 2012; Sinel'nikova et al., 2013). Since persons with epilepsy normally present with acute seizures as opposed to status epilepticus, our acute ECS studies may model human seizures with higher validity than SE or chronic stimulation protocols (by design, these tend to model epileptogenesis rather than acute seizures). It remains unclear for now what the role of microglial changes is in deciding the differential outcomes after the seizures from each model. Since ECS in rodents is a near-perfectly valid model for ECT in humans, our present data may point to a potential role in ECT's effects, although ECT in the clinic is administered chronically and no mood-stabilizing effects have been shown after single ECT sessions. Further research (including chronic treatments and experiments on mouse models of depression) are needed to elucidate whether the observed microglial response extends to ECT as used in the clinic.

In conclusion, we describe here a state of microglial "activation" in the mouse hippocampal area CA1*sr* one day after a single electroconvulsive shock-evoked seizure. Surprisingly, the observed microglial changes partially overlapped those seen after epileptogenic status epilepticus seizures. We posit that the changes present in the response to both models could represent a "signature" of maximal seizures in hippocampal microglia, with little sensitivity to the degree of damage or

ensuing epileptogenesis. Repeated ECS in mice is a near-perfect model of electroconvulsive therapy (ECT) in humans: as such, our results also raise a potential role for microglial changes in mediating either ECT's established benefits (anti-depressant/mood-stabilizing) or its equally well-known deleterious effects (confusion or amnesia).

850
851

852 REFERENCES

853

854 Ali I, Chugh D, Ekdahl CT (2015) Role of fractalkine–CX3CR1 pathway in seizure-
855 induced microglial activation, neurodegeneration, and neuroblast production in the
856 adult rat brain. Neurobiology of Disease 74:194–203.

857

858 Al- Muhtasib N, Sepulveda- Rodriguez A, Vicini S, Forcelli PA (2018) Neonatal
859 phenobarbital exposure disrupts GABAergic synaptic maturation in rat CA1
860 neurons. Epilepsia 59:333–344.

861

862 Alves M, Gomez- Villafuertes R, Delanty N, Farrell MA, O'Brien DF,
863 Miras- Portugal M, Hernandez M, Henshall DC, Engel T (2017) Expression and
864 function of the metabotropic purinergic P2Y receptor family in experimental seizure
865 models and patients with drug- refractory epilepsy. Epilepsia.

866

867 Amhaoul H, Ali I, Mola M, Eetveldt A, Szewczyk K, Missault S, Bielen K, Kumar-
868 Singh S, Rech J, Lord B, Ceusters M, Bhattacharya A, Dedeurwaerdere S (2016)
869 P2X7 receptor antagonism reduces the severity of spontaneous seizures in a
870 chronic model of temporal lobe epilepsy. Neuropharmacology 105:175–185.

871

872 Arisi GM, Foresti ML, Katki K, Shapiro LA (2015) Increased CCL2, CCL3, CCL5,
873 and IL-1β cytokine concentration in piriform cortex, hippocampus, and neocortex
874 after pilocarpine-induced seizures. Journal of Neuroinflammation 12:1–7.

875

876 Avignone E, Lepleux M, Angibaud J, Nägerl UV (2015) Altered morphological
877 dynamics of activated microglia after induction of status epilepticus. J
878 Neuroinflamm 12:202.

879

880 Avignone E, Ulmann L, Levavasseur F, Rassendren F, Audinat E (2008) Status
881 Epilepticus Induces a Particular Microglial Activation State Characterized by
882 Enhanced Purinergic Signaling. The Journal of Neuroscience 28:9133–9144.

883

884 AVMA (2013) AVMA Guidelines for the Euthanasia of Animals: 2013 Edition.

885

886 Basar K, Eren-Kocak E, Ozdemir H, Ertugrul A (2013) Effects of Acute and Chronic
887 Electroconvulsive Shocks on Glycogen Synthase Kinase 3[beta] Level and
888 Phosphorylation in Mice. The Journal of ECT 29:261.

889

890 Beamer E, Fischer W, Engel T (2017) The ATP-Gated P2X7 Receptor As a Target
891 for the Treatment of Drug-Resistant Epilepsy. Frontiers in Neuroscience 11:21.

892

893 Becker AJ (2017) Animal models of acquired epilepsy: insights into mechanisms of
894 human epileptogenesis. Neuropathology and Applied Neurobiology.

895

896 Bosco DB, Zheng J, Xu Z, Peng J, Eyo UB, Tang K, Yan C, Huang J, Feng L, Wu
897 G, Richardson JR, Wang H, Wu L-J (2018) RNAseq analysis of hippocampal
898 microglia after kainic acid-induced seizures. Mol Brain 11:34.

899

900 Bozzi Y, Caleo M (2016) Epilepsy, Seizures, and Inflammation: Role of the C-C
901 Motif Ligand 2 Chemokine. DNA and Cell Biology 35:257–260.
902
903 Cerri C, Genovesi S, Allegra M, Pistillo F, Püntener U, Guglielmotti A, Perry HV,
904 Bozzi Y, Caleo M (2016) The Chemokine CCL2 Mediates the Seizure-enhancing
905 Effects of Systemic Inflammation. The Journal of Neuroscience 36:3777–3788.
906
907 Chen Z, Duan R, Quezada H, Mix E, Nennesmo I, Adem A, Winblad B, Zhu J
908 (2005) Increased microglial activation and astrogliosis after intranasal
909 administration of kainic acid in C57BL/6 mice. Journal of Neurobiology 62:207–218.
910
911 Chen Z, Jalabi W, Hu W, Park H-J, Gale JT, Kidd GJ, Bernatowicz R, Gossman
912 ZC, Chen JT, Dutta R, Trapp BD (2014) Microglial displacement of inhibitory
913 synapses provides neuroprotection in the adult brain. Nature Communications
914 5:4486.
915
916 Cho K-O, Lybrand ZR, Ito N, Brulet R, Tafacory F, Zhang L, Good L, Ure K, Kernie
917 SG, Birnbaum SG, Scharfman HE, Eisch AJ, Hsieh J (2015) Aberrant hippocampal
918 neurogenesis contributes to epilepsy and associated cognitive decline. Nature
919 Communications 6:6606.
920
921 Conti G, Gale K, Kondratyev A (2009) Immunohistochemical evaluation of the
922 protein expression of nerve growth factor and its TrkA receptor in rat limbic regions
923 following electroshock seizures. Neuroscience Research 65:201–209.
924

925 Covolan L, Mello L (2000) Temporal profile of neuronal injury following pilocarpine
926 or kainic acid-induced status epilepticus. Epilepsy research 39:133–152.
927
928 Davalos D, Grutzendler J, Yang G, Kim JV, Zuo Y, Jung S, Littman DR, Dustin ML,
929 Gan W-BB (2005) ATP mediates rapid microglial response to local brain injury in
930 vivo. Nature neuroscience 8:752–758.
931
932 de Biase LM, Schuebel KE, Fusfeld ZH, Jair K, Hawes IA, Cimbro R, Zhang H-Y,
933 Liu Q-R, Shen H, Xi Z-X, Goldman D, Bonci A (2017) Local Cues Establish and
934 Maintain Region-Specific Phenotypes of Basal Ganglia Microglia. Neuron 95:341-
935 356.e6.
936
937 Devanand D, Dwork A, Hutchinson E, Bolwig T, Sackeim H (1994) Does ECT alter
938 brain structure? Am J Psychiat 151:957–970.
939
940 Devinsky O, Vezzani A, Najjar S, Lanerolle NC, Rogawski MA (2013) Glia and
941 epilepsy: excitability and inflammation. Trends in Neurosciences 36:174–184.
942
943 Dyrvig M, Hansen HH, Christiansen SH, Woldbye D, Mikkelsen JD, Lichota J
944 (2012) Epigenetic regulation of Arc and c-Fos in the hippocampus after acute
945 electroconvulsive stimulation in the rat. Brain Research Bulletin 88:507–513.
946
947 Engel T, Gomez-Villafuertes R, Tanaka K, Mesuret G, Sanz-Rodriguez A, Garcia-
948 Huerta P, Miras-Portugal TM, Henshall DC, Diaz-Hernandez M (2012) Seizure
949 suppression and neuroprotection by targeting the purinergic P2X7 receptor during

950 status epilepticus in mice. The FASEB Journal:1616–1628.
951
952 Eyo UB, Bispo A, Liu J, chika Sabu, Wu R, DiBona VL, Zheng J, Murugan M,
953 Zhang H, Tang Y, Wu L-J (2018) The GluN2A Subunit Regulates Neuronal NMDA
954 receptor-Induced Microglia-Neuron Physical Interactions. Scientific Reports 8:828.
955
956 Eyo UB, Murugan M, Wu L (2017) Microglia–Neuron Communication in Epilepsy.
957 Glia 65:5–18.
958
959 Eyo UB, Peng J, Murugan M, Mo M, Lalani A, Xie P, Xu P, Margolis DJ, Wu L-J
960 (2016a) Regulation of Physical Microglia-Neuron Interactions by Fractalkine
961 Signaling after Status Epilepticus. Eneuro 3:ENEURO.0209-16.2016.
962
963 Eyo UB, Peng J, Murugan M, Mo M, Lalani A, Xie P, Xu P, Margolis DJ, Wu L-JJ
964 (2016b) Regulation of Physical Microglia-Neuron Interactions by Fractalkine
965 Signaling after Status Epilepticus. eNeuro 3.
966
967 Eyo UB, Peng J, Swiatkowski P, Mukherjee A, Bispo A, Wu L-J (2014) Neuronal
968 Hyperactivity Recruits Microglial Processes via Neuronal NMDA Receptors and
969 Microglial P2Y12 Receptors after Status Epilepticus. The Journal of Neuroscience
970 34:10528–10540.
971
972 Fordyce CB, Jagasia R, Zhu X, Schlichter LC (2005) Microglia Kv1.3 channels
973 contribute to their ability to kill neurons. The Journal of neuroscience : the official
974 journal of the Society for Neuroscience 25:7139–7149.

975

976 Foresti ML, Arisi GM, Katki K, Montañez A, nchez R, Shapiro LA (2009) Chemokine
977 CCL2 and its receptor CCR2 are increased in the hippocampus following
978 pilocarpine-induced status epilepticus. Journal of Neuroinflammation 6:1–11.

979

980 Frankel W, Taylor L, Beyer B, Tempel B, White H (2001) Electroconvulsive
981 thresholds of inbred mouse strains. Genomics 74:306–312.

982

983 Fu R, Shen Q, Xu P, Luo J, Tang Y (2014) Phagocytosis of Microglia in the Central
984 Nervous System Diseases. Molecular Neurobiology 49:1422–1434.

985

986 Gorter JA, van Vliet EA, Aronica E (2015) Status epilepticus, blood–brain barrier
987 disruption, inflammation, and epileptogenesis. Epilepsy & Behavior 49:13–16.

988

989 Group TU (2003) Efficacy and safety of electroconvulsive therapy in depressive
990 disorders: a systematic review and meta-analysis. The Lancet 361:799–808.

991

992 Hammond TR, Dufort C, Dissing-Olesen L, Giera S, Young A, Wysoker A, Walker
993 AJ, Gergits F, Segel M, Nemesh J, Marsh SE, Saunders A, Macosko E, Ginhoux F,
994 Chen J, Franklin R, Piao X, McCarroll SA, Stevens B (2018) Single-Cell RNA
995 Sequencing of Microglia throughout the Mouse Lifespan and in the Injured Brain
996 Reveals Complex Cell-State Changes. Immunity.

997

998 Haynes SE, Hollopeter G, Yang G, Kurpius D, Dailey ME, Gan W-B, Julius D
999 (2006) The P2Y12 receptor regulates microglial activation by extracellular

1000 nucleotides. Nature Neuroscience 9:1512–1519.
1001
1002 Henshall DC, Engel T (2015) P2X purinoceptors as a link between hyperexcitability
1003 and neuroinflammation in status epilepticus. Epilepsy & Behavior 49:8–12.
1004
1005 Hevers W, Lüddens H (2002) Pharmacological heterogeneity of γ-aminobutyric acid
1006 receptors during development suggests distinct classes of rat cerebellar granule
1007 cells in situ. Neuropharmacology 42:34–47.
1008
1009 Hong S, Beja-Glasser VF, Nfonoyim BM, Frouin A, Li S, Ramakrishnan S, Merry
1010 KM, Shi Q, Rosenthal A, Barres BA, Lemere A, Selkoe DJ, Stevens B (2016)
1011 Complement and microglia mediate early synapse loss in Alzheimer mouse
1012 models. Science 352:aad8373.
1013
1014 Hsieh TF, Simler S, Vergnes M, Gass P, Marescaux C, Wiegand SJ, Zimmermann
1015 M, Herdegen T (1998) BDNF Restores the Expression of Jun and Fos Inducible
1016 Transcription Factors in the Rat Brain Following Repetitive Electroconvulsive
1017 Seizures. Exp Neurol 149:161–174.
1018
1019 Ilie A, Raimondo JV, Akerman CJ (2012) Adenosine release during seizures
1020 attenuates GABAA receptor-mediated depolarization. The Journal of neuroscience :
1021 the official journal of the Society for Neuroscience 32:5321–5332.
1022
1023 INGVAR M (1986) Cerebral Blood Flow and Metabolic Rate during Seizuresa. Ann
1024 Ny Acad Sci 462:194–206.

1025

1026 Iyengar SS, LaFrancois JJ, Friedman D, Drew LJ, Denny CA, Burghardt NS, Wu
1027 MV, Hsieh J, Hen R, Scharfman HE (2015) Suppression of Adult Neurogenesis
1028 Increases the Acute Effects of Kainic Acid. Experimental Neurology 264:135–149.

1029

1030 Jansson L, Wennström M, Johanson A, Tingström A (2009) Glial cell activation in
1031 response to electroconvulsive seizures. Progress in Neuro-Psychopharmacology
1032 and Biological Psychiatry 33:1119–1128.

1033

1034 Jarvis MF, Khakh BS (2009) ATP-gated P2X cation-channels. Neuropharmacology
1035 56:208–215.

1036

1037 Ji R-R, Schlaepfer TE, Aizenman CD, Epstein CM, Qiu D, Huang JC, Rupp F
1038 (1998) Repetitive transcranial magnetic stimulation activates specific regions in rat
1039 brain. Proc National Acad Sci 95:15635–15640.

1040

1041 Jiang L, Mackenzie A, North R, Surprenant A (2000) Brilliant blue G selectively
1042 blocks ATP-gated rat P2X(7) receptors. Molecular pharmacology 58:82–88.

1043

1044 Jimenez-Pacheco A, Diaz-Hernandez M, Arribas-Blázquez M, Sanz-Rodriguez A,
1045 Olivos-Oré LA, Artalejo AR, Alves M, Letavic M, Miras-Portugal M, Conroy RM,
1046 Delanty N, Farrell MA, O'Brien DF, Bhattacharya A, Engel T, Henshall DC (2016)
1047 Transient P2X7 Receptor Antagonism Produces Lasting Reductions in
1048 Spontaneous Seizures and Gliosis in Experimental Temporal Lobe Epilepsy. The
1049 Journal of neuroscience : the official journal of the Society for Neuroscience

36:5920–5932.

Jimenez- Pacheco A, Mesuret G, Sanz- Rodriguez A, Tanaka K, Mooney C, Conroy R, Miras- Portugal M, Diaz- Hernandez M, Henshall DC, Engel T (2013) Increased neocortical expression of the P2X7 receptor after status epilepticus and anticonvulsant effect of P2X7 receptor antagonist A- 438079. Epilepsia 54:1551–1561.

Jinno S, Kosaka T (2008) Reduction of Iba1-expressing microglial process density in the hippocampus following electroconvulsive shock. Experimental Neurology 212:440–447.

Jung S, Aliberti J, Graemmel P, Sunshine M, Kreutzberg GW, Sher A, Littman DR (2000) Analysis of Fractalkine Receptor CX3CR1 Function by Targeted Deletion and Green Fluorescent Protein Reporter Gene Insertion. Molecular and Cellular Biology 20:4106–4114.

Kalozoumi G, Kel-Margoulis O, Vafiadaki E, Greenberg D, Bernard H, Soreq H, Depaulis A, Sanoudou D (2018) Glial responses during epileptogenesis in Mus musculus point to potential therapeutic targets. PLOS ONE 13:e0201742.

Kettenmann H, Hanisch U-KK, Noda M, Verkhratsky A (2011) Physiology of microglia. 91:461–553.

Khakh B, Burnstock G, Kennedy C, King B, North R, Séguéla P, Voigt M,

1075 Humphrey P (2001) International union of pharmacology. XXIV. Current status of
1076 the nomenclature and properties of P2X receptors and their subunits. Pharmacol
1077 Rev 53:107–118.
1078
1079 Kim J-E, Ryu H, Kang T-C (2013) Status Epilepticus Induces Vasogenic Edema via
1080 Tumor Necrosis Factor-α/ Endothelin-1-Mediated Two Different Pathways. Plos
1081 One 8:e74458.
1082
1083 Klein P et al. (2017) Commonalities in epileptogenic processes from different acute
1084 brain insults: Do they translate? Epilepsia.
1085
1086 Klement W, Garbelli R, Zub E, Rossini L, Tassi L, Girard B, Blaquiere M, Bertaso F,
1087 Perroy J, de Bock F, Marchi N (2018) Seizure progression and inflammatory
1088 mediators promote pericytosis and pericyte-microglia clustering at the
1089 cerebrovasculature. Neurobiol Dis 113:70–81.
1090
1091 Li B, Suemaru K, Cui R, Araki H (2007) Repeated electroconvulsive stimuli have
1092 long-lasting effects on hippocampal BDNF and decrease immobility time in the rat
1093 forced swim test. Life Sciences 80:1539–1543.
1094
1095 Liang X, Samways DS, Wolf K, Bowles EA, Richards JP, Bruno J, Dutertre S,
1096 DiPaolo RJ, Egan TM (2015) Quantifying Ca2+ Current and Permeability in ATP-
1097 gated P2X7 Receptors. Journal of Biological Chemistry 290:7930–7942.
1098
1099 Löscher W (2011) Critical review of current animal models of seizures and epilepsy

used in the discovery and development of new antiepileptic drugs. Seizure 20:359–368.

Lovatt D, Xu Q, Liu W, Takano T, Smith NA, Schnermann J, Tieu K, Nedergaard M (2012) Neuronal adenosine release, and not astrocytic ATP release, mediates feedback inhibition of excitatory activity. Proceedings of the National Academy of Sciences 109:6265–6270.

Madry C, Arancibia-Cárcamo LI, Kyrargyri V, Chan VT, Hamilton NB, Attwell D (2018) Effects of the ecto-ATPase apyrase on microglial ramification and surveillance reflect cell depolarization, not ATP depletion. Proceedings of the National Academy of Sciences 115:201715354.

Marchi N, Angelov L, Masaryk T, Fazio V, Granata T, Hernandez N, Hallene K, Diglaw T, Franic L, Najm I, Janigro D (2007) Seizure- Promoting Effect of Blood–Brain Barrier Disruption. Epilepsia 48:732–742.

McCarroll SA, Stevens B (2018) microgliasinglecell.com. Microglia Single Cell Atlas of Health and Injury Available at: http://www.microgliasinglecell.com/.

Menteyne A, Levavasseur F, Audinat E, Avignone E (2009) Predominant Functional Expression of Kv1.3 by Activated Microglia of the Hippocampus after Status epilepticus. Plos One 4:e6770.

Morinobu S, Strausbaugh H, Terwilliger R, Duman RS (1997) Regulation of c- Fos

and NGF1- A by antidepressant treatments. Synapse 25:313–320.

Murase K, Ryu PD, Randic M (1989) Excitatory and inhibitory amino acids and peptide-induced responses in acutely isolated rat spinal dorsal horn neurons. Neurosci Lett 103:56–63.

Nimmerjahn A, Kirchhoff F, Helmchen F (2005) Resting Microglial Cells Are Highly Dynamic Surveillants of Brain Parenchyma in Vivo. Science 308:1314–1318.

Nimmerjahn A, Kirchhoff F, Kerr JN, Helmchen F (2004) Sulforhodamine 101 as a specific marker of astroglia in the neocortex in vivo. Nature Methods 1:nmeth706.

Ohsawa K, Irino Y, Sanagi T, Nakamura Y, Suzuki E, Inoue K, Kohsaka S (2010) P2Y12 receptor-mediated integrin-beta1 activation regulates microglial process extension induced by ATP. Glia 58:790–801.

Orr AG, Orr AL, Li X-J, Gross RE, Traynelis SF (2009) Adenosine A2A receptor mediates microglial process retraction. Nature Neuroscience 12:nn.2341.

Orzi F, Zoli M, Passarelli F, Ferraguti F, Fieschi C, Agnati L (1990) Repeated electroconvulsive shock increases glial fibrillary acidic protein, ornithine decar□ylase, somatostatin and cholecystokinin immunoreactivities in the hippocampal formation of the rat. Brain Res 533:223–231.

Parkhurst CN, Yang G, Ninan I, Savas JN, Yates JR, Lafaille JJ, Hempstead BL,

1150 Littman DR, Gan W-B (2013) Microglia Promote Learning-Dependent Synapse
1151 Formation through Brain-Derived Neurotrophic Factor. Cell 155:1596–1609.
1152
1153 Patterson KP, Brennan GP, Curran M, Kinney-Lang E, Dubé C, Rashid F, Ly C,
1154 Obenaus A, Baram TZ (2015) Rapid, Coordinate Inflammatory Responses after
1155 Experimental Febrile Status Epilepticus: Implications for Epileptogenesis. Eneuro
1156 2:ENEURO.0034-15.2015.
1157
1158 Pearce PS, Friedman D, Lafrancois JJ, Iyengar SS, Fenton AA, Maclusky NJ,
1159 Scharfman HE (2014) Spike-wave discharges in adult Sprague-Dawley rats and
1160 their implications for animal models of temporal lobe epilepsy. Epilepsy & behavior :
1161 E&B 32:121–131.
1162
1163 Plata-Salamán CR, Ilyin SE, Turrin NP, Gayle D, Flynn MC, Romanovitch AE, Kelly
1164 ME, Bureau Y, Anisman H, McIntyre DC (2000) Kindling modulates the IL-1β
1165 system, TNF-α, TGF-β1, and neuropeptide mRNAs in specific brain regions.
1166 Molecular Brain Research 75:248–258.
1167
1168 Pollard H, Charriaut-Marlangue C, Cantagrel S, Represa A, Robain O, Moreau J,
1169 Ben-Ari Y (1994) Kainate-induced apoptotic cell death in hippocampal neurons.
1170 Neuroscience 63:7–18.
1171
1172 Racine R (1972) Modification of seizure activity by electrical stimulation. II. Motor
1173 seizure. Electroencephalography and clinical neurophysiology 32:281–294.
1174

1175 Ravizza T, Vezzani A (2005) Status epilepticus induces time-dependent neuronal
1176 and astrocytic expression of interleukin-1 receptor type I in the rat limbic system.
1177 Neuroscience 137:301–308.
1178
1179 Rettenbeck ML, von Rüden E-L, Bienas S, Carlson R, Stein VM, Tipold A,
1180 Potschka H (2015) Microglial ROS production in an electrical rat post-status
1181 epilepticus model of epileptogenesis. Neurosci Lett 599:146–151.
1182
1183 Sabilallah M, Fontanaud P, Linck N, Boussadia B, Peyroutou R, Lasgouzes T,
1184 Rassendren FA, Marchi N, Hirbec HE (2016) Evidence for Status Epilepticus and
1185 Pro-Inflammatory Changes after Intranasal Kainic Acid Administration in Mice.
1186 PLOS ONE 11:e0150793.
1187
1188 Schafer DP, Lehrman EK, Stevens B (2013) The “quad- partite” synapse:
1189 Microglia- synapse interactions in the developing and mature CNS. Glia.
1190
1191 Schartz ND, Herr SA, Madsen L, Butts SJ, Torres C, Mendez LB, Brewster AL
1192 (2016) Spatiotemporal profile of Map2 and microglial changes in the hippocampal
1193 CA1 region following pilocarpine-induced status epilepticus. Scientific Reports
1194 6:24988.
1195
1196 Schmued LC, Stowers CC, Scallet AC, Xu L (2005) Fluoro-Jade C results in ultra
1197 high resolution and contrast labeling of degenerating neurons. Brain Research
1198 1035:24–31.
1199

1200 Scorza F, Arida R, Priel M, Calderazzo L, Cavalheiro E, de das Cruzes U, do de
1201 Paulo U, do de Paulo U, do de Paulo U, do de Paulo U (2002) Glucose utilisation
1202 during status epilepticus in an epilepsy model induced by pilocarpine: a qualitative
1203 study. Arq Neuro-psiquiat 60:198–203.
1204
1205 Scott A (1995) Does ECT alter brain structure? Am J Psychiat 152:1403a – 1403.
1206
1207 Shapiro LA, Wang L, Ribak CE (2008) Rapid astrocyte and microglial activation
1208 following pilocarpine- induced seizures in rats. Epilepsia 49:33–41.
1209
1210 Sinel'nikova V, Shubina L, Gol'tyaev M, Loseva E, Kichigina V (2013) Detection of
1211 c-Fos Expression in the Brains of Animals with a Pilocarpine Model of Temporal
1212 Lobe Epilepsy. Neurosci Behav Physiology 43:1084–1091.
1213
1214 Stevens B, Allen NJ, Vazquez LE, Howell GR, Christopherson KS, Nouri N,
1215 Micheva KD, Mehalow AK, Huberman AD, Stafford B, Sher A, Litke AM, Lambris
1216 JD, Smith SJ, John S, Barres BA (2007) The Classical Complement Cascade
1217 Mediates CNS Synapse Elimination. Cell 131:1164–1178.
1218
1219 Tian D-SS, Peng J, Murugan M, Feng L-JJ, Liu J-LL, Eyo UB, Zhou L-JJ,
1220 Mogilevsky R, Wang W, Wu L-JJ (2017) Chemokine CCL2-CCR2 Signaling
1221 Induces Neuronal Cell Death via STAT3 Activation and IL-1β Production after
1222 Status Epilepticus. The Journal of neuroscience : the official journal of the Society
1223 for Neuroscience 37:7878–7892.
1224

1225 Toyomitsu E, Tsuda M, Yamashita T, Tozaki-Saitoh H, Tanaka Y, Inoue K (2012)
1226 CCL2 promotes P2X4 receptor trafficking to the cell surface of microglia. Purinergic
1227 Signalling 8:301–310.
1228
1229 Tremblay M-È, Lowery RL, Majewska AK (2010) Microglial Interactions with
1230 Synapses Are Modulated by Visual Experience. PLoS Biology 8:e1000527.
1231
1232 Tremblay M-È, Stevens B, Sierra A, Wake H, Bessis A, Nimmerjahn A (2011) The
1233 Role of Microglia in the Healthy Brain. The Journal of Neuroscience 31:16064–
1234 16069.
1235
1236 Turski W, Cavalheiro E, Bortolotto Z, Mello L, hwarz, Turski L (1984) Seizures
1237 produced by pilocarpine in mice: a behavioral, electroencephalographic and
1238 morphological analysis. Brain research 321:237–253.
1239
1240 Ulmann L, Levavasseur F, Avignone E, Peyroutou R, Hirbec H, Audinat E,
1241 Rassendren F (2013) Involvement of P2X4 receptors in hippocampal microglial
1242 activation after status epilepticus. Glia 61:1306–1319.
1243
1244 van Buel EM, Sigrist H, Seifritz E, Fikse L, Bosker FJ, Schoevers RA, Klein HC,
1245 Pryce CR, Eisel UL (2017) Mouse repeated electroconvulsive seizure (ECS) does
1246 not reverse social stress effects but does induce behavioral and hippocampal
1247 changes relevant to electroconvulsive therapy (ECT) side-effects in the treatment of
1248 depression. PLOS ONE 12:e0184603.
1249

van Vliet E, da Araújo CS, Redeker S, van Schaik R, Aronica E, Gorter J (2007) Blood–brain barrier leakage may lead to progression of temporal lobe epilepsy. Brain 130:521–534.

Vasek MJ et al. (2016) A complement–microglial axis drives synapse loss during virus-induced memory impairment. Nature 534:538–543.

Verkhratsky A, Noda M (2014) General Physiology and Pathophysiology of Microglia. :47–60.

Vezzani A, French J, Bartfai T, Baram TZ (2011) The role of inflammation in epilepsy. Nature Reviews Neurology 7:31.

Weiner RD, Reti IM (2017) Key updates in the clinical application of electroconvulsive therapy. International Review of Psychiatry:1–9.

Weinhard L, di Bartolomei G, Bolasco G, Machado P, Schieber NL, Neniskyte U, Exiga M, Vadisiute A, Raggioli A, Schertel A, Schwab Y, Gross CT (2018) Microglia remodel synapses by presynaptic trogocytosis and spine head filopodia induction. Nature Communications 9:1228.

Wieraszko A, Goldsmith G, Seyfried TN (1989) Stimulation-dependent release of adenosine triphosphate from hippocampal slices. Brain Res 485:244–250.

Wu P, Phillis J (1978) Distribution and release of adenosine triphosphate in rat

brain. Neurochem Res 3:563–571.

Wyatt-Johnson SK, Herr SA, Brewster AL (2017) Status Epilepticus Triggers Time-Dependent Alterations in Microglia Abundance and Morphological Phenotypes in the Hippocampus. Frontiers in Neurology 8:700.

Zhang B, Zou J, Han L, Beeler B, Friedman JL, Griffin E, Piao Y, Rensing NR, Wong M (2018) The specificity and role of microglia in epileptogenesis in mouse models of tuberous sclerosis complex. Epilepsia 59:1796–1806.

Zhao X, Liao Y, Morgan S, Mathur R, Feustel P, Mazurkiewicz J, Qian J, Chang J, Mathern GW, Adamo MA, Ritaccio AL, Gruenthal M, Zhu X, Huang Y (2018) Noninflammatory Changes of Microglia Are Sufficient to Cause Epilepsy. Cell Reports 22:2080–2093.

Zou J, Zhang B, Gutmann DH, Wong M (2017) Postnatal reduction of tuberous sclerosis complex 1 expression in astrocytes and neurons causes seizures in an age- dependent manner. Epilepsia 58:2053–2063.

FIGURE LEGENDS

Figure 1. ECS did not affect density of microglia and did not cause neuronal degeneration in mouse CA1 24 hours after seizures.

A. Representative maximal intensity projections from immunofluorescence image showing $CX_3CR1\text{-}GFP^+$ microglia in green and $NeuN^+$ neurons in red in CA1 (*str. pyramidale* = left of dashed line; *str. radiatum* = right of dashed line) of control (top) and ECS (bottom) mice 24 hours after seizures.

B. Density of microglia in CA1*sr* microglia per 10^6 μm^3 of CA1*sr* volume. Control animals had 26.69±2.9 which was not significantly different from ECS animals that had 27.59±2.7.

C. Number of FluoroJade C positive cells per field imaged (320μm x 240μm). Control and ECS-exposed animals have significantly lower degenerating cell densities in CA1 than SE-exposed animals: 4.2±0.36 for controls (N=9) and 3.6±0.54 for ECS animals (N=5), compared to 16.3±1.5 for SE animals (N=7).

Figure 2. ECS did not affect spontaneous motility of microglia in mouse CA1*sr* 24 hours after seizures.

A,B. Representative time-coded images (t=0 in red, t=20 minutes in green, overlap in yellow) of CA1*sr* fields (**A**) or single cells (**B**) from slices from control (right/top) and ECS (left/bottom) treated animals.

C. ECS had no effect on mean Extension Index (area of extensions/area of retractions) after 20 minutes of imaging under baseline conditions: 1.085±0.041 for control slices and 1.067±0.05 for ECS slices.

Figure 3. Unlike Status Epilepticus, ECS did not cause morphological activation of CA1*sr* microglia.

A. Representative binarized images of individual traced microglia from control, ECS or SE animals.

B. SE, but not ECS, significantly decreased the number of 3D Sholl crossings in hippocampal microglia (for radii between 2μm and 33μm).

C. SE significantly decreased the total number of branch points per cell, while ECS had no significant effect.

D. SE significantly decreased the total filament length per cell, while ECS had no significant effect.

E. SE significantly decreased the average number of primary branches, while ECS had no significant effect.

Figure 4. ECS increased expression of CCL2 without affecting *Tnf or the* microglial marker *Tmem119*.

A. Hippocampi were lysed 24h after seizures, and the ratio of CCL2 to total protein was measured in the lysates by ELISA and BCA assay. ECS and SE similarly induced a significant upregulation of relative CCL2 expression.

B. After MACS isolation 24h after ECS or sham ECS, microglial RNA samples were studied by hydrolysis probe-based qPCR. Relative fold change for each transcript assayed (the microglial marker *Tmem119*, the pro-inflammatory cytokine *Tnf* and the chemokine *Ccl2*) was determined by the $2^{-\Delta\Delta Ct}$ method, normalizing to *Actb* levels. We observed significantly higher relative expression of *Ccl2* mRNA in ECS microglial samples, and no significant changes elsewhere.

Figure 5. ECS, like Status Epilepticus, potentiated the ATP-responsive motility of microglial processes in acute hippocampal slices.

A,B. Representative maximal intensity projections of confocal zt-stacks showing the time-course of the microglial response (in green) to 3mM ATP in a patch pipette (in red) in acute hippocampal slices from control (**A**) ECS (**B**) and SE (**C**) animals.

D. ECS and SE similarly increased the average process velocity during the microglial response to 3mM ATP.

E. ECS-induced enhancement of microglial responsive motility is concentration-dependent: there was a small but significant difference in the responses to 1mM ATP, while the responses to 10mM were not significantly different.

Figure 6. ECS had no effect on intrinsic electrophysiological properties of CA1*sr* microglia.

A. Representative photomicrograph showing GFP-labeled microglia superimposed with a 60X DIC image of the hippocampal slice.

B. Current density-voltage relation in microglia was unchanged after ECS. Current amplitudes were measured at steady state during 500ms voltage steps. Data are shown as mean±SEM.

C,D,E. ECS did not affect microglial Resting Membrane Potential (**C**), Input Resistance (**D**) or Membrane Capacitance (**E**).

Figure 7. ECS enhanced P2X7 current density in CA1*sr* microglia.

A, B. Representative voltage-clamp traces showing the currents induced by local application of 1mM ATP (black bar) in normal or 0CaMg aCSF (yellow bar), in microglia in slices from sham (**A**) vs. ECS (**B**) animals. Cells were held at Vm=−60mV, with 500ms ramps from −120mV to +50mV every 10s.

C, D. Peak current density (current amplitude/cell capacitance, pA/pF) of 1mM ATP-evoked currents in normal (**C**) and divalent cation-free/0CaMg aCSF (**D**) at Vm=−60mV. ECS resulted in significantly increased current densities under both recording conditions. Panels on the right represent the average ATP-induced current/voltage relation obtained by subtracting the I/V curve obtained before from that obtained during the ATP application. As is expected for P2X-mediated currents, the I/V relation is linear and reverses around 0mV.

E. Peak current density (current amplitude/cell capacitance, pA/pF) of 1mM ATP-evoked currents in normal aCSF at Vm=−60mV, with or without preincubation in the specific P2X7 antagonist Brilliant Blue G (BBG). BBG significantly reduced the current density evoked by 1mM ATP in normal aCSF in ECS cells only.

F. Peak current density (pA/pF) of 1mM ATP-evoked currents in divalent cation-free/0CaMg aCSF at Vm=−60mV, with or without BBG preincubation. BBG significantly reduced the current density evoked by 1mM ATP in 0CaMg aCSF in both control and ECS cells.

Figure 8. ECS did not change microglial expression of purinergic receptor transcripts.

After MACS isolation 24h after ECS or sham ECS, microglial RNA samples were studied by hydrolysis probe-based qPCR. Relative fold change for each purinergic receptor transcript assayed (the ionotropic receptors *P2rx1*, *P2rx4* and

1395 *P2rx7* and the metabotropic receptors *P2ry6* and *P2ry12*) was determined by the $2^{-\Delta\Delta Ct}$
1396 method, normalizing to *Actb* levels. ECS did not have statistically significant
1397 effects on the expression of any of the studied genes.
1398

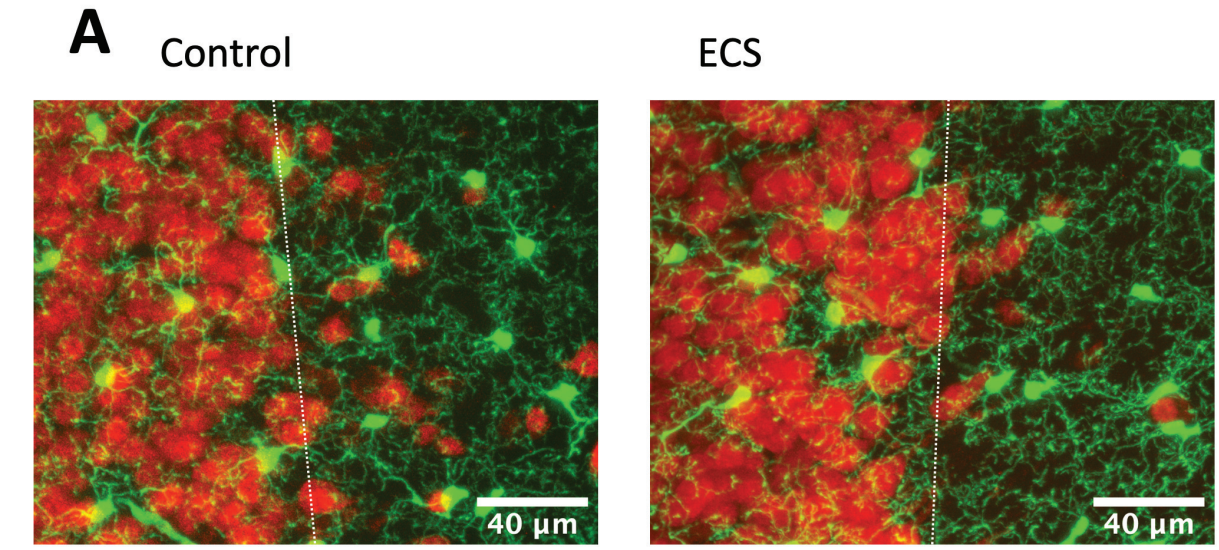

Cornu Ammonis 1 *stratum pyramidale* and *stratum radiatum*
NeuN (neurons, mostly clustered pyramidal cells in CA1*sp*)
CX_3CR1-GFP (microglia)